Research Article Vol. 60, No. 18 / 20 June 2021 / Applied Optics 5345

applied optics

Design and experimental demonstration of 8-QAM coherent free-space optical communication using amplitude compensation and phase recovery

Lin Li,[1,*] Tianwen Geng,[1] Zhiyong Wu,[1] Shijie Gao,[1] and Xueliang Li[1]

[1]Changchun Institute of Optics, Fine Mechanics and Physics, Chinese Academy of Sciences, Dongnanhu Road 3888, Changchun 130033, China
*Corresponding author: lilin920329@126.com

Received 7 April 2021; revised 24 May 2021; accepted 24 May 2021; posted 26 May 2021 (Doc. ID 427122); published 14 June 2021

In this paper, a new, to the best of our knowledge, scheme is proposed to mitigate the atmospheric turbulence effect in coherent free-space optical (FSO) communications with 8-quadrature amplitude modulation by employing amplitude compensation and phase recovery. The amplitude compensation and phase recovery algorithm in the scheme can significantly improve system performance without acquiring instantaneous channel state information or probability density function of a turbulence model. Numerical studies show that the bit error rate of the proposed scheme is four orders of magnitude lower than that of the system without any algorithm over a lognormal turbulence channel with normalized standard deviation of irradiance $\sigma = 0.25$ and phase noise with normalized variance $\sigma_\phi^2 = 0.07$, when the frequency offset $f_o = 20$ MHz, combined linewidth $\Delta f = 10$ kHz, and average signal-to-noise ratio $\gamma = 20$ dB. Experiments are also carried out to investigate the performance of the scheme, and the results prove its superiority. Hence, this scheme can contribute to practical realization of the FSO system.

https://doi.org/10.1364/AO.427122

1. INTRODUCTION

In recent years, there has been growing interest in free-space optical (FSO) communication for scientific, commercial, and military applications since it supports a quick and inexpensive setup, unlicensed spectrum, and excellent security [1–6]. Traditional FSO systems are mainly based on on–off keying (OOK) modulation. This is because the OOK system is simple and easy to build [7–10]. However, the effectivity of an OOK system for high data rate relay is relatively low. With the rapid increase in data traffic, the capacity of the FSO system is urgently desired to be improved [11,12].

To obtain a high data rate, quadrature amplitude modulation (QAM) is studied for the FSO system. The FSO system using QAM can encode information in both phase and amplitude of the carrier, but the system also suffers from atmospheric turbulence [13–15]. To study the performance of a QAM FSO system in atmospheric turbulence, a lot of research has been done. In [16], the theoretical bit error rate (BER) performance of the amplify-and-forward (AF) relay-added QAM FSO system over a weak atmospheric turbulence channel was analyzed. Peppas and Datsikas [17] derived approximate closed-form expressions for the average symbol error probability of a FSO communication link using subcarrier intensity modulation with general-order rectangular QAM over atmospheric turbulence channels. Vu *et al.* [18] analyzed the performance of FSO communication systems using rectangular QAM and an avalanche photodiode (APD) receiver over atmospheric turbulence channels. The BER of the M-ary QAM modulation technique for a FSO link under turbulent atmospheric conditions was investigated in [19]. In [20], Escribano and Wagemakers studied QAM-multipulse pulse-position modulation (MPPM) in turbulence-free FSO channels, and provided accurate analytical expressions for its error probabilities and simplified expressions for estimation of error probabilities. In [21], the performance of a dual-hop variable gain AF mixed radio frequency/FSO system with QAM was analyzed in detail.

In the meantime, many schemes have been proposed to improve the performance of QAM FSO systems. For example, Chen *et al.* [22] experimentally demonstrated a high-speed air–water transmission employing a 32-quadrature amplitude modulation-orthogonal frequency division multiplexing (32-QAM-OFDM) modulated 520 nm laser diode. A novel 1.12 Tbps dense wavelength division multiplexing system for 16-QAM FSO communication was given in [23]. Wang *et al.* [24] proposed a high-speed visible light communication system using quadrature amplitude modulation-discrete multi-tone (QAM-DMT) modulation based on digital zero-padding and a differential receiver. Zhang *et al.* [25] designed and experimentally demonstrated a two-path parallel scheme for m-QAM-OFDM transmission in FSO communications.

In this study, an 8-QAM FSO communication system with amplitude compensation and phase recovery is proposed. The

amplitude compensation algorithm and phase recovery algorithm in the scheme can improve the quality of the signal and effectively suppress the influence of atmospheric turbulence, combined linewidth [spectral width of the transmitter and local oscillator (LO)], and frequency offset. Numerical studies and experiments show that such a system provides good BER performance without acquiring the instantaneous channel state information (CSI) or probability density function (PDF) of the channel model.

The remainder of the paper is organized as follows. In Section 2, the channel model is introduced. The system architecture is given in Section 3. The amplitude compensation and phase recovery algorithm are introduced and analyzed in Section 4. Numerical and experiment results are given in Section 5. Finally, some concluding remarks are provided in Section 6.

2. CHANNEL MODEL

In FSO systems, one of the remaining impediments is atmospheric scintillation, which can cause fading. In this paper, a lognormally distributed fading channel is considered. The PDF of atmospheric turbulence induced fading is given as

$$f(I)=\frac{1}{\sqrt{8\pi}I\sigma}\exp\left\{-\frac{\left[\ln(I)+2\sigma^2\right]^2}{8\sigma^2}\right\},\ I>0. \tag{1}$$

The log-amplitude variance σ^2 can be represented by Rytov variance σ_R^2 for a plane wave as

$$\sigma^2=\frac{{\sigma_R}^2}{4}=\frac{1}{4}(1.23C_n^2k^{7/6}L^{11/6}), \tag{2}$$

where C_n^2 is the atmospheric structure constant, $k=2\pi/\lambda$ is the wave number, and L is the propagation distance [26]. For a FSO system near the ground, the atmospheric structure constant varies from 10^{-17} $\mathrm{m}^{-2/3}$ to 10^{-13} $\mathrm{m}^{-2/3}$ according to atmospheric turbulence conditions [27].

FSO systems also suffer from atmospheric turbulence induced phase noise φ_n, which obeys zero-mean Gaussian statistics. Supposing a Kolmogorov spectrum of turbulence, the classical statistics of phase noise variance are extended to consider modal compensation of atmospheric phase distortion. In modal compensation, the residual phase noise variance σ_ϕ^2 is usually expressed by Zernike polynomials [28,29]. Then the residual phase variance after modal compensation of J Zernike terms can be expressed as

$$\sigma_\phi^2=C_J\left(\frac{D}{r_0}\right)^{5/3}, \tag{3}$$

where D is the aperture diameter of the receive antenna, r_0 is the Fried parameter, and C_J is the coefficient of Zernike–Kolmogoroff residual errors. The coefficient $C_J=1.0299$ in the phase variance σ_ϕ^2 assumes that no terms are corrected by a receiver employing active modal compensation [30]. For plane waves, r_0 can be expressed as $r_0=1.68(C_n^2Lk^2)^{-3/5}$ [31].

3. SYSTEM ARCHITECTURE

The block diagram of the proposed system is given in Fig. 1. At the transmitter, a three-bit binary information sequence $a_3a_2a_1$ is first supplied to an electrical 8-QAM modulator that gives in-phase and quadrature-phase components of the signal shown in the constellation diagram. The constellation of the 8-QAM signal can be considered as the combination of two quadrature phase-shift keying (QPSK) constellations with different modulation indices and initial phases φ_i. Then the in-phase and quadrature-phase components are sent to a Mach–Zehnder modulator (MZM) to modulate the laser beam. After being amplified by an erbium-doped fiber amplifier (EDFA), the modulated beam is sent to an atmospheric channel through the optical antenna. The signal sent by the transmitter can be written as

$$S(t)=E_SA(t)\exp\left[j(\omega_ct+\varphi_n)\right], \tag{4}$$

where E_s and ω_c are the amplitude and angular frequency of the carrier wave, respectively, $\varphi_n\in\left\{-\frac{3\pi}{4},-\frac{\pi}{2},-\frac{\pi}{4},0,\frac{\pi}{4},\frac{\pi}{2},\frac{3\pi}{4},\pi\right\}$ is the modulated phase. $A(t)=\sum_{n=-\infty}^{\infty}a_ng(t-nT_S),a_n\in\{C_1,C_2\}$ is the modulated amplitude, and C_1 and C_2 denote the modulation indices. $g(t)$ is the shaping pulse, and T_S denotes the symbol interval.

At the receiver, the signal received by the optical antenna is amplified by an EDFA. Then the received signal beats with the LO in a 2 * 4 90° optical hybrid, and the output signals are detected by two balanced photodetectors. The states of polarization (SOPs) of the LO and received signal are assumed to be the same by using a polarization controller (PC). After that, the electrical in-phase and quadrature signals are sampled and processed by the amplitude compensation and phase recovery algorithm given in Section 4. Finally, an electrical 8-QAM demodulator is used to demodulate the signal.

The received signal suffers from geometric loss between the transmitting antenna and receiving antenna, which can be expressed as

$$G_L=20\log_{10}\left(\frac{D}{D_T+\theta_{\mathrm{div}}L}\right), \tag{5}$$

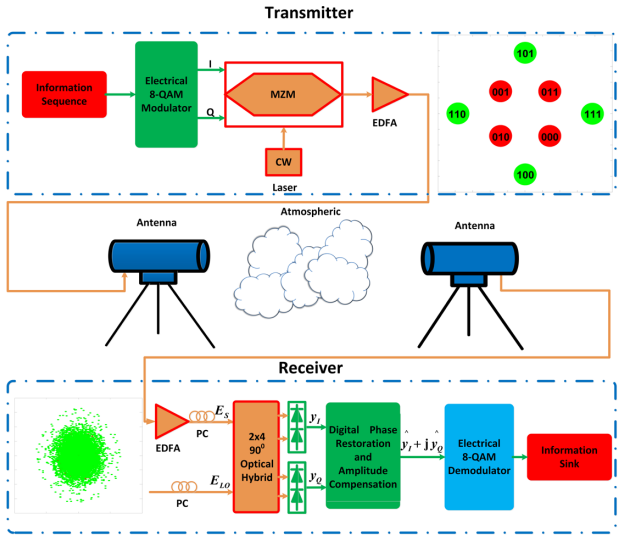

Fig. 1. Architecture of the system.

where D_T is the aperture diameter of the transmitting antenna, and θ_{div} is the divergence angle. The received signal is also affected by great attenuation of the atmospheric channel. Normally, the power loss of the received signal is regarded as constant and can be compensated for by the EDFA in the receiver. In the meantime, the received signal suffers from atmospheric turbulence induced fading, which can be expressed as a multiplicative stationary random process $I(t)$ and phase fluctuations that obey zero-mean Gaussian statistics with variance σ_ϕ^2. As mentioned in Section 2, we assume that $I(t)$ follows a lognormal distribution with normalized standard deviation of irradiance σ.

At the receiver, after the balanced photodetectors, the signals can be written as

$$\begin{aligned} y_I(nT_S) &= RE_S E_{\mathrm{LO}} I(nT_S) A(nT_S) \cos[(\omega_c - \omega_{\mathrm{LO}})nT_S \\ &\quad + \varphi_n + \varphi_s(nT_S) + \varphi_{ps}(nT_S)] + n_1(nT_S), \\ y_Q(nT_S) &= RE_S E_{\mathrm{LO}} I(nT_S) A(nT_S) \sin[(\omega_c - \omega_{\mathrm{LO}})nT_S \\ &\quad + \varphi_n + \varphi_s(nT_S) + \varphi_{ps}(nT_S)] + n_2(nT_S), \end{aligned} \tag{6}$$

where R is the photodetector responsivity, E_{LO} and ω_{LO} are the amplitude and angular frequency of the LO, respectively, $\varphi_s(t)$ is the phase noise caused by atmospheric turbulence, $\varphi_{ps}(nT_S)$ denotes the carrier phase in reference to the LO phase, and we assume that the phase difference $\varphi_{ps}(t+T_S) - \varphi_{ps}(t)$ in a symbol interval T_S follows a Gaussian distribution with a variance $\sigma_p^2 = 4\pi\Delta f T_S$, where Δf is the combined linewidth of the transmitter and LO. $n_1(t)$ and $n_2(t)$ represent additive white Gaussian noise due to thermal noise and shot noise in the receiver with total power σ_g^2. For convenience, we set R, E_{LO}, and E_S as one in the rest of the paper.

4. AMPLITUDE COMPENSATION AND PHASE RECOVERY ALGORITHM

A. Amplitude Compensation Algorithm

After the balanced photodetectors, the amplitude compensation algorithm is used to process the electrical in-phase and quadrature signals. The diagram of the algorithm is given in Fig. 2. As shown in the picture, to obtain the impact of atmospheric turbulence on signal amplitude, the sum of squares of the in-phase and quadrature signals is first given as

$$\begin{aligned} &{y_I}^2(nT_S) + {y_Q}^2(nT_S) \\ &= I^2(nT_S)A^2(nT_S) + {n_1}^2(nT_S) + {n_2}^2(nT_S) \\ &\quad + 2I(nT_S)A(nT_S)\cos[(\omega_c - \omega_{\mathrm{LO}})nT_S + \varphi_n \\ &\quad + \varphi_s(nT_S) + \varphi_{ps}(nT_S)]\, n_1(nT_S) \\ &\quad + 2I(nT_S)A(nT_S)\sin[(\omega_c - \omega_{\mathrm{LO}})nT_S + \varphi_n \\ &\quad + \varphi_s(nT_S) + \varphi_{ps}(nT_S)]\, n_2(nT_S). \end{aligned} \tag{7}$$

Then the results of ${y_I}^2(nT_S) + {y_Q}^2(nT_S)$ are summed and averaged over N neighbor symbols. When the average length N is large enough, we can assume that

$$\begin{aligned} &\lim_{N\to\infty} \sum_{n=1}^{N} \frac{{y_I}^2(nT_S) + {y_Q}^2(nT_S)}{N} \\ &= E[{y_I}^2(nT_S) + {y_Q}^2(nT_S)] \\ &= E[I^2(nT_S)]E[A^2(nT_S)] + 2\sigma_g^2, \end{aligned} \tag{8}$$

where the noise power σ_g^2 can be easily obtained by using pilot symbols, and $E[A^2(nT_S)]$ can be regarded as a known constant in a certain system.

For a practical lasercom system, the atmospheric time constant (which is of the order of 1 ms) would exceed the data symbol durations (500 ps, for example) by many orders of magnitude. The atmospheric turbulence induced fading can be seen as a constant over a frame with a suitable length N (10^6, for example). Therefore, we have

$$\begin{aligned} \frac{1}{I_g} &= \sqrt{\frac{1}{E[A^2(t)]}\left(\lim_{K\to\infty}\sum_{n=1}^{K}\frac{{y_I}^2(nT_S) + {y_Q}^2(nT_S)}{K} - 2\sigma_g^2\right)}^{-1} \\ &\approx \frac{1}{I(nT_S)}, \end{aligned} \tag{9}$$

where $I(nT_S)$ denotes the amplitude fluctuation caused by atmospheric turbulence on the received signal. I_g is the estimation of $I(nT_S)$, which is obtained from K neighbor symbols by the amplitude compensation algorithm.

After that, the signals $y_I(nT_S)$ and $y_Q(nT_S)$ are processed with the amplitude compensation to mitigate the impact of atmospheric turbulence on signal amplitude. The output can be expressed by

$$\begin{aligned} R(nT_S) &= y_I'(nT_S) + \mathrm{j}y_Q'(nT_S) = \frac{y_I(nT_S) + \mathrm{j}y_Q(nT_S)}{I_g} \\ &\approx A(nT_S)\exp\{\mathrm{j}[(\omega_c - \omega_{\mathrm{LO}})nT_S + \varphi_n + \varphi_s(nT_S) \\ &\quad + \varphi_{ps}(nT_S)]\} + \frac{n_1(nT_S) + \mathrm{j}n_2(nT_S)}{I(nT_S)}. \end{aligned} \tag{10}$$

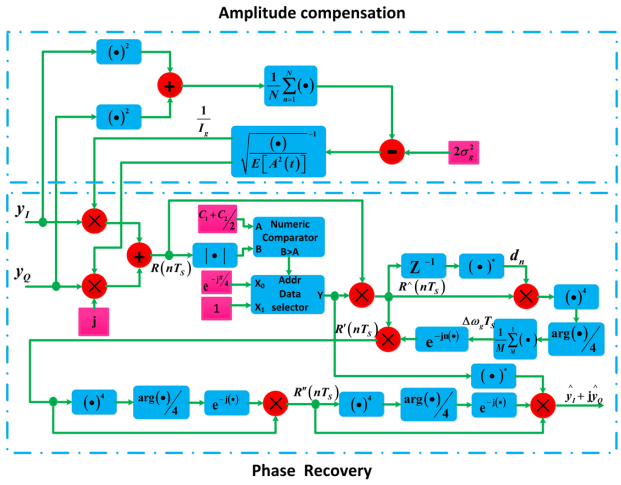

Fig. 2. Diagram of the amplitude compensation and phase recovery algorithm.

B. Phase Recovery Algorithm

The output signal of the amplitude compensation algorithm is then sent into a phase recovery unit, as shown in Fig. 2. First, the absolute value of $R(nT_S)$ is calculated and compared with the threshold between the inner and outer "rings" in the constellation to determine the initial phase of the signal. The threshold is set as $C_1 + C_2/2$. Then the initial phase information is removed by a data selector and multiplier to eliminate the influence of initial phase on the phase recovery algorithm. The output can be expressed by

$$R^{\wedge}(nT_S) = R(nT_S)\exp[-\mathrm{j}\varphi_i(nT_S)]. \tag{11}$$

To reduce the influence of frequency offset, the output $R^{\wedge}(nT_S)$ is first multiplied by $\{R^{\wedge}[(n-1)T_S]\}^*$, which is the conjugate of the output that delays a symbol interval. For our system, when average SNR is large enough, we have

$$\begin{aligned} d_n = {} & R^{\wedge}(nT_S) \times \{R^{\wedge}[(n-1)T_S]\}^* \approx A(nT_S)A[(n-1)T_S] \\ & \times \exp\{\mathrm{j}[\Delta\omega T_S + \varphi_n - \varphi_{n-1} - \varphi_i(nT_S) + \varphi_i((n-1)T_S) \\ & + \varphi_s(nT_S) - \varphi_s((n-1)T_S) + \varphi_{ps}(nT_S) - \varphi_{ps}((n-1)T_S)]\}, \end{aligned} \tag{12}$$

where $\Delta\omega = \omega_S - \omega_{\mathrm{LO}}$. After that, the fourth power function $(\bullet)^4$ is used to remove the modulated phase, since $4\{\varphi_n - \varphi_{n-1} - \varphi_i(nT_S) + \varphi_i[(n-1)T_S]\} = 2\pi m$ (m is integer). When average SNR is large enough, the output signal can be approximately written as

$$\begin{aligned} {d^4}_n \approx {} & A^4(nT_S)A^4[(n-1)T_S]\exp\{4j[\Delta\omega T_S + \varphi_s(nT_S) \\ & - \varphi_s((n-1)T_S) + \varphi_{ps}(nT_S) - \varphi_{ps}((n-1)T_S)]\}. \end{aligned} \tag{13}$$

Then ${d^4}_n$ is further processed by the operation $\arg(\bullet)/4$ as

$$\begin{aligned} \frac{\arg({d^4}_n)}{4} \approx {} & \Delta\omega T_S + \varphi_s(nT_S) - \varphi_s[(n-1)T_S] \\ & + \varphi_{ps}(nT_S) - \varphi_{ps}[(n-1)T_S], \end{aligned} \tag{14}$$

where $\varphi_s(nT_S)$, $\varphi_s[(n-1)T_S]$, and $\varphi_{ps}(nT_S) - \varphi_{ps}[(n-1)T_S]$ obey zero-mean Gaussian statistics.

To obtain the frequency offset, the results of Eq. (14) are summed and averaged over M neighbor symbols. When the average length M is large enough, we can assume that

$$\Delta\omega_g T_S = \lim_{M\to\infty}\sum_{n=1}^{M}\frac{\arg({d^4}_n)}{4M} \approx \Delta\omega T_S, \tag{15}$$

where $\Delta\omega_g$ is the estimation of angular frequency offset $\Delta\omega = 2\pi f_0$ obtained from M neighbor symbols. Then $\Delta\omega_g$ is used to process $R^{\wedge}(nT_S)$ as

$$\begin{aligned} R'(nT_S) = {} & R^{\wedge}(nT_S)\exp(-\mathrm{j}n\Delta\omega_g T_S) \\ \approx {} & A(nT_S)\exp\{\mathrm{j}[\varphi_n - \varphi_i(nT_S) + \varphi_s(nT_S) + \varphi_{ps}(nT_S)]\}. \end{aligned} \tag{16}$$

To estimate the phase noise caused by atmospheric turbulence and the combined linewidth of the transmitter and LO, $R'(nT_S)$ is processed by the fourth power function $(\bullet)^4$ to remove the modulated phase, since $4[\varphi_n - \varphi_i(nT_S)] = 2\pi m$ (m is integer). The output signal can be approximately written as

$$[R'(nT_S)]^4 \approx A^4(nT_S)\exp\{4j[\varphi_s(nT_S) + \varphi_{ps}(nT_S)]\}. \tag{17}$$

The estimation of the phase noise can be expressed by

$$\varphi_{gs}(nT_S) + \varphi_{gps}(nT_S) = \frac{\arg\left\{[R'(nT_S)]^4\right\}}{4}, \tag{18}$$

where $\varphi_{gs}(nT_S)$ is the estimation of the phase noise caused by atmospheric turbulence, and $\varphi_{gps}(nT_S)$ denotes the estimation of the phase noise caused by the combined linewidth of the transmitter and LO. Then the estimation of phase noise is used to process $R'(nT_S)$ as

$$R''(nT_S) = R'(nT_S)\exp\left\{-\mathrm{j}[\varphi_{gs}(nT_S) + \varphi_{gps}(nT_S)]\right\}. \tag{19}$$

To refine the phase recovery, as shown in Fig. 2, $R''(nT_S)$ is further processed by the fourth power function $(\bullet)^4$ and the operation $\arg(\bullet)/4$ as

$$\varphi_{ge}(nT_S) = \frac{\arg\{[R''(nT_S)]^4\}}{4}, \tag{20}$$

where φ_{ge} denotes the estimation of the remaining phase noise.

Finally, initial phase information is given back, and the output of the signal processed by the amplitude compensation and phase recovery algorithm can be expressed by

$$\begin{aligned} \hat{y}_I + \mathrm{j}\hat{y}_Q = {} & R''(nT_S)\exp\{-\mathrm{j}[\varphi_{ge}(nT_S) - \varphi_i(nT_S)]\} \\ \approx {} & A(nT_S)\exp(\mathrm{j}\varphi_n). \end{aligned} \tag{21}$$

To achieve amplitude compensation, $2K$ square operations, K-1 additions, two divisions, one multiplication, and one subtraction are needed in the algorithm. In the meantime, the algorithm needs $2M+5$ multiplications, $M+2$ fourth power operations, $M+2$ calculating angle operations, $M+3$ divisions, and M-1 additions to realize phase recovery.

5. NUMERICAL AND EXPERIMENT RESULTS

Simulations and experiments are carried out to investigate the performance of the proposed scheme. As we discussed in Section 2, the optical turbulence parameters for our study are set as in Table 1.

The symbol rate of the system is set as 1 Gbps. The length N of a frame with 200 pilot symbols is set as 10^6. We also set $C_1 = (\sqrt{6} - \sqrt{2})/2$, $C_2 = 1$ during the simulations and experiments. As mentioned in Section 3, C_1 and C_2 denote the modulation indices of the inner and outer rings in the constellation.

Simulations are performed with the commercial software tool MATLAB, and the noise bandwidth is assumed to be equal to the data rate in the simulations.

The constellation diagrams of the signal at different stages in the receiver of the system using amplitude compensation and phase recovery during the simulation are shown in Fig. 3, where the frequency offset $f_0 = 20$ MHz and the combined linewidth of the transmitter and LO $\Delta f = 10$ kHz. The optical

Table 1. Parameters Used in the Study

Parameter	Value I	Value II	Value III	Value IV
Wavelength λ	1550 nm	1550 nm	1550 nm	1550 nm
Aperture diameter D	5 cm	8 cm	5 cm	5 cm
Atmospheric structure constant C_n^2	10^{-16} $m^{-2/3}$	10^{-16} $m^{-2/3}$	10^{-16} $m^{-2/3}$	10^{-15} $m^{-2/3}$
Transmission distance L	14 km	14 km	30 km	14 km
Atmospheric coherent diameter r_0	25.5 cm	25.5 cm	16.2 cm	6.4 cm
Log-amplitude standard deviation σ	0.25	0.25	0.50	0.79
Phase noise variance σ_ϕ^2	0.07	0.15	0.15	0.68

turbulence parameters are set as value I in Table 1; the length K to obtain I_g and the length M to obtain $\Delta\omega_g$ are set as 200 and 800, respectively. Monte Carlo computer simulations with 10^8 trials are used to obtain the simulated constellation diagrams. In Fig. 3, we can see that the atmospheric turbulence, frequency offset, and the combined linewidth seriously affect the quality of the signal, and the constellation of the received signal is randomly distributed (a). The inphase-quadrature (IQ) plot of the signal is split into two rings after amplitude compensation (b). Then the constellation of the signal is improved obviously after frequency offset estimation (c) and further improved after phase noise estimation (d). It shows that the proposed scheme can significantly improve the signal quality.

The following simulated BER results are also obtained by the Monte Carlo computer simulations. The simulation process is given as follows. For the limitation of the computer's random access memory (RAM), first, 10^6 frames of data are created and stored in a file on the local hard disk. Then the data are read from the file and sent by different systems with different turbulences, given in Table 1. Finally, the simulated BERs can be achieved by comparing the final output data of the receivers with the data in the file.

As can be seen in Fig. 4, the simulated BERs versus average electrical SNR at the receiver for the 8-QAM system using amplitude compensation and phase recovery with different K and M are plotted. We set $f_0 = 20$ MHz, $\Delta f = 10$ KHz, and the optical turbulence parameters are set as value I in Table 1. In Fig. 4, it can be seen that the BER of the system improves with the increase in K and M. This is because the appropriate increase in K and M can make the estimation of atmospheric turbulence induced fading and angular frequency offset more precise.

In Fig. 5, the simulated BERs of the 8-QAM system using amplitude compensation and phase recovery with different frequency offsets versus average electrical SNR at the receiver are plotted, where $\Delta f = 10$ KHz, $K = 200$, and $M = 800$. The optical turbulence parameters are also set as value I in Table 1 during the simulation. Note that the rise in frequency offset leads to significant degradation in the error performance of the system. It shows that although the proposed scheme can

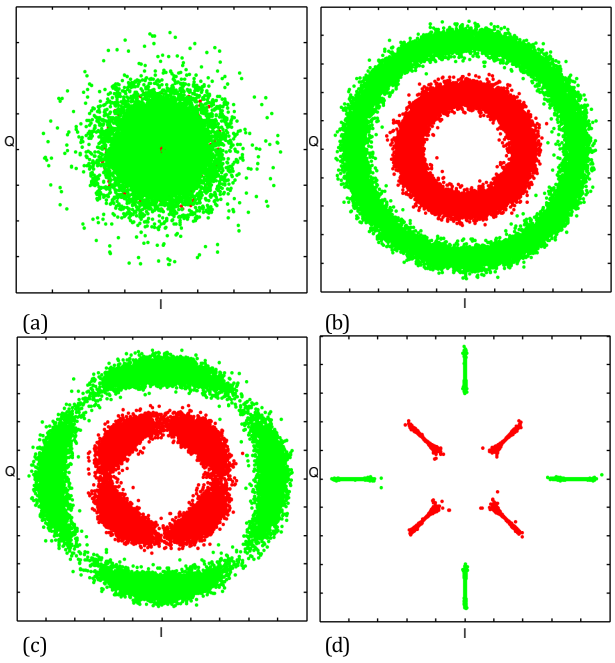

Fig. 3. Simulated constellation diagrams of the signal at different stages in the receiver of the system using amplitude compensation and phase recovery. (a) After balanced photodetectors, (b) after amplitude compensation, (c) after frequency offset estimation, and (d) after phase noise estimation.

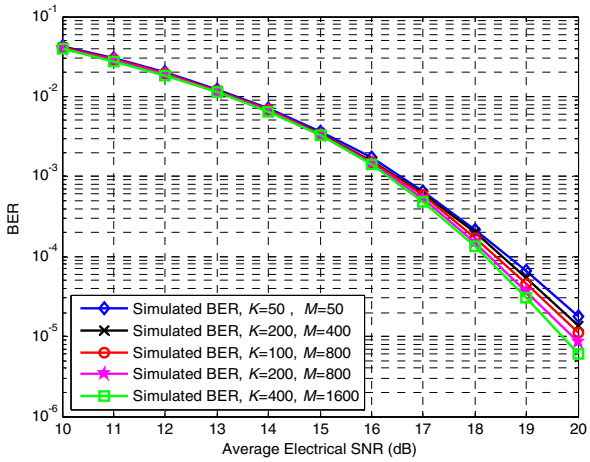

Fig. 4. Simulated BERs of the 8-QAM system using amplitude compensation and phase recovery with different K and M.

reduce the impact of frequency offset on the BER of the system, it cannot completely eliminate the frequency offset.

As can be seen in Fig. 6, the simulated BERs of the 8-QAM system using amplitude compensation and phase recovery with different combined linewidth versus average electrical SNR at the receiver are plotted, where $f_0 = 20$ MHz, $K = 200$, and $M = 800$. We set the optical turbulence parameters as value I in Table 1. Note that the performance loss of SNR is less than 1 dB due to the increase of the combined linewidth of the transmitter and LO at a BER of 10^{-3}. It shows that the proposed scheme can mitigate the influence of combined linewidth on the BER of the system.

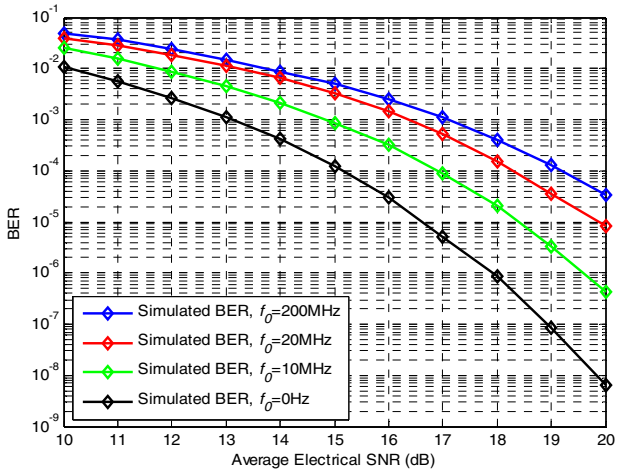

Fig. 5. Simulated BERs of the 8-QAM system using amplitude compensation and phase recovery with different frequency offsets.

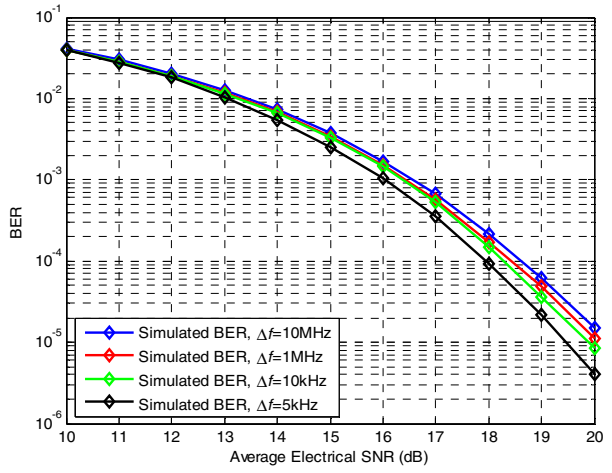

Fig. 6. Simulated BERs of the 8-QAM system using amplitude compensation and phase recovery with different combined linewidths.

The simulated BERs versus average electrical SNR at the receiver for the 8-QAM system using amplitude compensation and phase recovery with different atmospheric turbulences are shown in Fig. 7. We set $f_0 = 20$ MHz, $\Delta f = 10$ KHz, $K = 200$, and $M = 800$. In Fig. 7, it can be seen that the error performance of the system degrades with the rise of log-amplitude standard deviation and phase noise variance. Combined with Table 1, it shows that transmission distance, atmospheric structure constant, and aperture diameter influence system performance.

In Fig. 8, the simulated BERs versus average electrical SNR at the receiver for different 8-QAM systems are plotted, where $f_0 = 20$ MHz, $\Delta f = 10$KHz, and the optical turbulence parameters are set as value I in Table 1. As can be seen in Fig. 8, the BER of the system with amplitude compensation is only slightly better than that of the system without any algorithm. This is due to the great influence of the frequency offset, combination linewidth, and atmospheric turbulence on signal phase. Compared with the system without any algorithm and the system with only amplitude compensation, the system with phase recovery has better BER performance. The proposed scheme

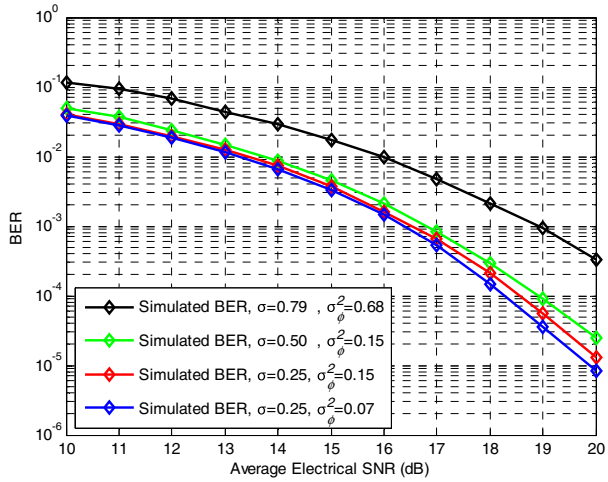

Fig. 7. Simulated BERs of the 8-QAM system using amplitude compensation and phase recovery with different atmospheric turbulences.

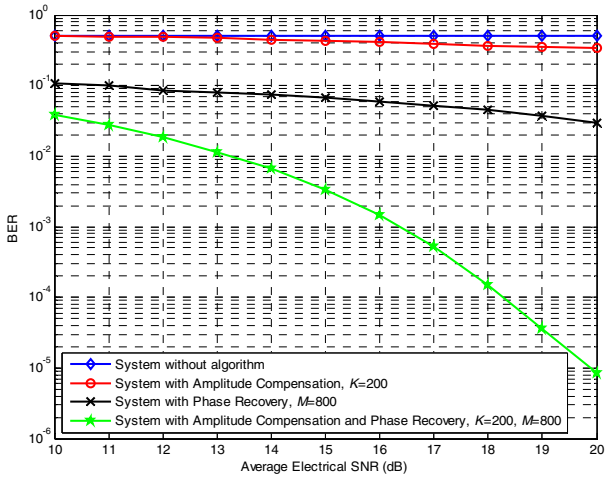

Fig. 8. Simulated BERs of different 8-QAM systems.

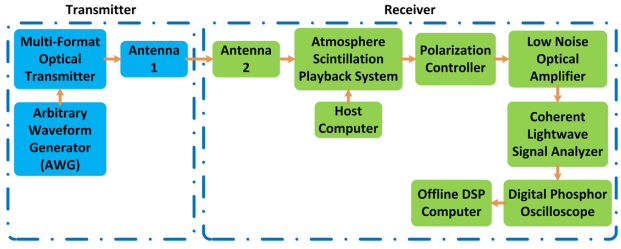

Fig. 9. Block diagram of the experimental setup.

further improves the error performance of the system and eliminates the error floor that appears in the large SNR regime. It is also seen in Fig. 8 that the BER of the proposed system is four orders of magnitude lower than that of the system without any algorithm, when the SNR is 20 dB.

The block diagram and the photo of the experimental setup are shown in Fig. 9 and Fig. 10, respectively. In the experiments, the generation and recovery of 8-QAM symbols are

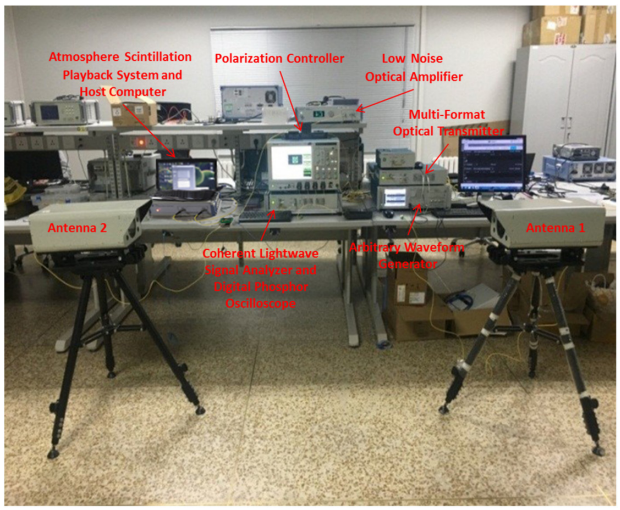

Fig. 10. Photo of the experimental setup.

both realized by off-line digital signal processing (DSP) using MATLAB.

At the transmitter, a pseudorandom binary sequence (PRBS) is first mapped into 8-QAM symbols. After that, the phase fluctuations caused by atmospheric turbulence are added to the symbols. Then the symbols are uploaded to an arbitrary waveform generator (AWG, Tektronix AWG70002A). The output signals of the AWG are sent to a multi-format optical transmitter (Tektronix OM5110) to modulate the laser beam. Finally, the modulated beam is sent to the receiver through optical antenna 1. The transmit power is set as 10dBm.

At the receiver, the modulated beam is received by optical antenna 2. The distance between antenna 1 and antenna 2 is 2 m. To make the optical antennas simple and compact, Galileo telescopes are used as antenna 1 and antenna 2. The aperture diameter and the divergence angle of the transmitting antenna are 2 cm and 1 mrad, respectively. The aperture diameter of the receiving antenna is 8 cm. An atmospheric scintillation playback system is designed to simulate the atmospheric turbulence induced amplitude fluctuation in the experiments. The block diagram and a photo of the atmosphere scintillation playback system are shown in Fig. 11 and Fig. 12, respectively. As shown in Fig. 11, it is composed of an Ethernet module, FPGA (FPGA), digital-to-analog converter (DAC) and variable optical attenuator (VOA). The system is controlled by the host computer through transmission control protocol/internet protocol (TCP/IP). The bandwidth of the system is 100 kHz, the attenuation accuracy is 0.1 dB, and the dynamic range is greater than 30 dB. Then the PC is used to keep the SOP of the LO and received signal consistent. To keep the frequency offset $f_0 = 20$ MHz, a feedback loop is used to maintain the laser bias and temperature of the transmitter and LO. The LO power is set as 14.5 dBm, and the combined linewidth of the transmitter and LO is measured to be 10 kHz according to the method described in [32]. The received signal and LO are beat in the coherent light wave signal analyzer (Tektronix OM4106D) and converted into electrical signal. After that, the output signal is sampled and recorded by the digital phosphor oscilloscope (Tektronix DPO73304D). Finally, the captured samples are processed by an offline DSP computer.

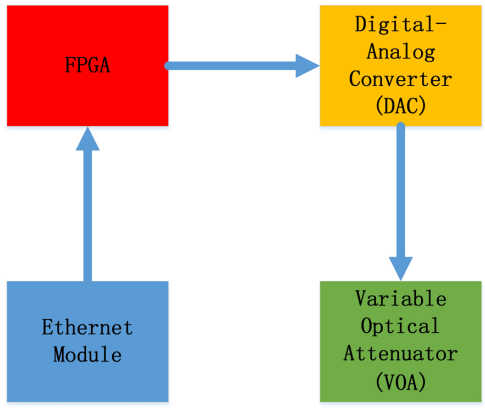

Fig. 11. Block diagram of the atmosphere scintillation playback system.

Fig. 12. Photo of the atmosphere scintillation playback system.

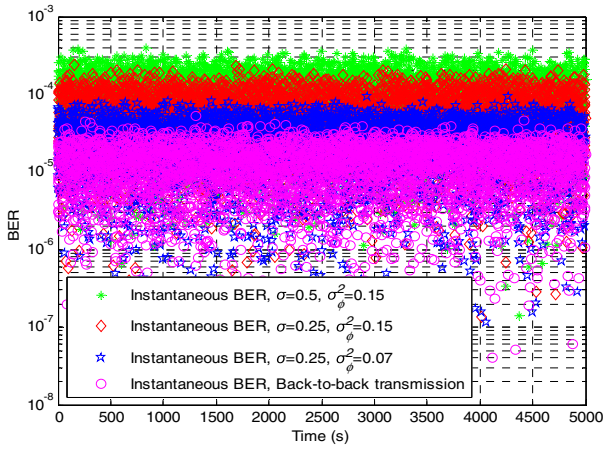

Fig. 13. Instantaneous BERs of the 8-QAM system using amplitude compensation and phase recovery with different atmospheric turbulences.

In offline processing, the instantaneous BERs of the systems are obtained by analyzing the BERs per second. The results of the experiments are given as follows.

In Fig. 13, the instantaneous BERs of the 8-QAM system using amplitude compensation and phase recovery with different atmospheric turbulences and back-to-back transmission are plotted, where $f_0 = 20$ MHz, $K = 200$, and $M = 800$. As can be seen in Fig. 13, the system with back-to-back transmission has better BER performance. The instantaneous BER of the system increases with the rise in normalized standard deviation of irradiance σ and variance of phase noise ${\sigma_\phi}^2$.

The instantaneous BERs of the 8-QAM system using amplitude compensation and phase recovery with different frequency offsets are shown in Fig. 14. We set $\sigma = 0.25$, ${\sigma_\phi}^2 = 0.07$, $K = 200$, and $M = 800$. In Fig. 14, it can be seen that the

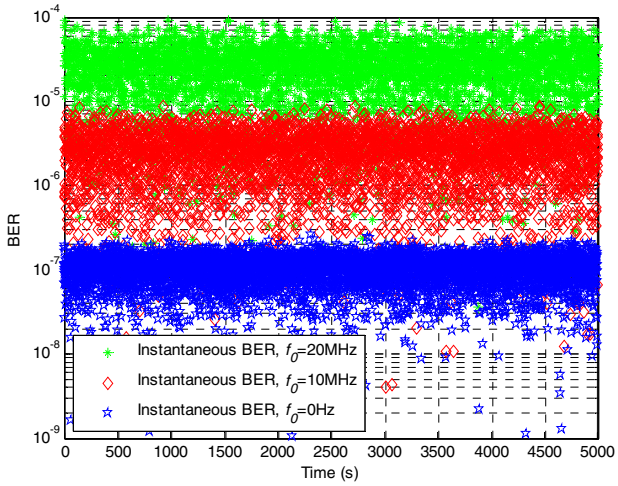

Fig. 14. Instantaneous BERs of the 8-QAM system using amplitude compensation and phase recovery with different frequency offsets.

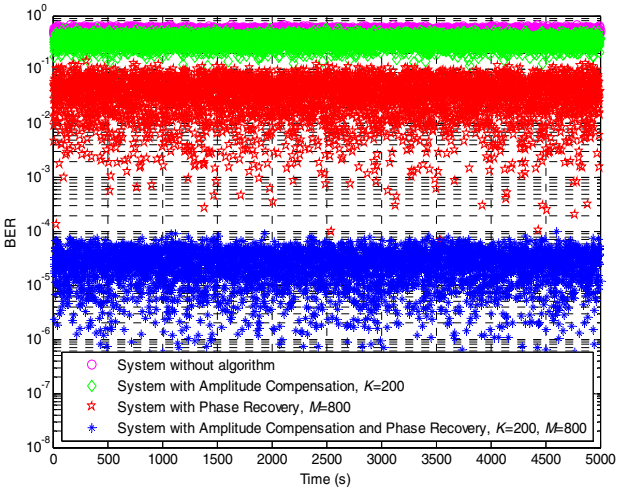

Fig. 15. Instantaneous BERs of different 8-QAM systems.

instantaneous BER also increases with the rise in frequency offset between the receiver and transmitter.

The instantaneous BERs of different 8-QAM systems are plotted in Fig. 15, where $f_0 = 20$ MHz, $\sigma = 0.25$, and $\sigma_\phi^2 = 0.07$. In Fig. 15, it can be seen that the BER of the system without any algorithm is the highest; the BERs of the system with amplitude compensation algorithm and the system with phase recovery algorithm are lower. The BER of the system using amplitude compensation and phase recovery is the lowest. Thus, compared with other systems, the proposed system has better instantaneous BER performance. Therefore, the system using amplitude compensation and phase recovery can effectively suppress the influence of atmospheric turbulence, combined linewidth, and frequency offset.

It can be seen from the above that the experimental results basically show agreement with the simulation results. The instantaneous BERs of the system given in Fig. 13 and the simulated BERs given in Fig. 7 show that the strength of turbulence will affect the BER performance of the system. From the experimental results and simulation results given in Figs. 14 and 5, it can be seen that the rise in frequency offset between the receiver and transmitter can seriously injure the BER performance of the system. The influence of the frequency offset can be mitigated by the scheme, but cannot be eliminated. Finally, both Figs. 15 and 8 prove the superiority of the proposed system.

6. CONCLUSION

In this paper, 8-QAM coherent FSO communication using amplitude compensation and phase recovery has been proposed. The principle of the proposed scheme is theoretically derived first. Then simulations and experiments are carried out. Results show that the systems can achieve good BER performance and effectively suppress the influence of atmospheric turbulence, combined linewidth, and frequency offset. Hence, the proposed scheme can contribute to the performance improvement of the FSO system and its practical realization.

Funding. Research Project of Scientific Research Equipment of Chinese Academy of Sciences (62001448).

Acknowledgment. The authors gratefully acknowledge the Optical Communication Laboratory of CIOMP for the use of their equipment. The authors wish to thank the anonymous reviewers for their valuable suggestions.

Disclosures. The authors declare no conflicts of interest.

Data Availability. Data underlying the results presented in this paper are not publicly available at this time but may be obtained from the authors upon reasonable request.

REFERENCES

1. Z. Huang, Z. Wang, M. Huang, W. Li, T. Lin, P. He, and Y. Ji, "Hybrid optical wireless network for future SAGO-integrated communication based on FSO/VLC heterogeneous interconnection," IEEE Photon. J. **9**, 1–11 (2017).
2. K. Li, J. Ma, L. Tan, S. Yu, and C. Zhai, "Performance analysis of fiber-based free-space optical communications with coherent detection spatial diversity," Appl. Opt. **55**, 4649–4656 (2016).
3. J. Gao and Y. Zhang, "Average capacity of ground-to-train wireless optical communication links in the non-Kolmogorov and gamma-gamma distribution turbulence with pointing errors," Opt. Commun. **358**, 147–153 (2016).
4. W. Lim, C. Yun, and K. Kim, "BER performance analysis of radio over free-space optical systems considering laser phase noise under gamma-gamma turbulence channels," Opt. Express **17**, 4479–4484 (2009).
5. J. Chen, Y. Huang, R. Cai, A. Zheng, Z. Yu, T. Wang, Z. Liu, and S. Gao, "Free-space communication turbulence compensation by optical phase conjugation," IEEE Photon. J. **12**, 1–11 (2020).
6. L. Yang, B. Zhu, J. Cheng, and J. F. Holzman, "Free-space optical communications using on–off keying and source information transformation," J. Lightwave Technol. **24**, 4750–4762 (2006).
7. D. H. Ai, H. D. Trung, and D. T. Tuan, "AF relay-assisted MIMO/FSO/QAM systems in gamma-gamma fading channels," in *3rd National Foundation for Science and Technology Development Conference on Information and Computer Science* (2016), pp. 147–152.
8. B. T. Vu, C. T. Truong, A. T. Pham, and N. T. Dang, "Performance of rectangular QAM/FSO systems using APD receiver over atmospheric turbulence channels," in *IEEE Region 10 Conference (TENCON)*, Cebu, Philippines, 2012, pp. 1–5.
9. T. V. Nguyen, A. T. H. Bui, N. T. Dang, and A. T. Pham, "Performance of SIM/S-QAM FSO systems with phase errors in gamma-gamma turbulence channels," in *International Conference on Information and Communication Technology Convergence* (2018), pp. 85–90.

10. J. Kaur, R. Miglani, J. S. Malhotra, and G. S. Gaba, "Performance analysis of M-ARY QAM modulated FSO links over turbulent AWGN channel," Int. J. Appl. Eng. Res. **10**, 35322–35327 (2015).
11. Z. Cao, X. Zhang, G. Osnabrugge, J. Li, I. M. Vellekoop, and A. M. J. Koonen, "Reconfigurable beam system for non-line-of-sight free-space optical communication," Light Sci. Appl. **8**, 69 (2019).
12. V. S. Rakesh and R. Singhal, "720-Mbps 64-QAM-OFDM SCM transmission over RGB-LED-based FSO communication system," in *13th International Conference on Wireless and Optical Communications Networks* (IEEE, 2016), pp. 1–5.
13. R. Jee and S. Chandra, "Performance analysis of WDM-free-space optical transmission system with M-QAM modulation under atmospheric and optical nonlinearities," in *International Conference on Microwave* (IEEE, 2016), pp. 41–44.
14. H. S. Khallaf, H. M. H. Shalaby, J. M. Garrido-Balsells, and S. Sampei, "Performance analysis of a hybrid QAM-MPPM technique over turbulence-free and gamma–gamma free-space optical channels," J. Opt. Commun. Netw. **9**, 161–171 (2017).
15. P. K. Jha, N. Kachare, K. Kalyani, and D. S. Kumar, "Performance analysis of FSO system with spatial diversity and relays for M-QAM over log-normal channel," arXiv:1709.05488, 1–17 (2017).
16. H. D. Trung, N. T. Hoa, N. H. Trung, and T. Ohtsuki, "A closed-form expression for performance optimization of subcarrier intensity QAM signals-based relay-added FSO systems with APD," Phys. Commun. **31**, 203–211 (2018).
17. K. P. Peppas and C. K. Datsikas, "Average symbol error probability of general-order rectangular quadrature amplitude modulation of optical wireless communication systems over atmospheric turbulence channels," J. Opt. Commun. Netw. **2**, 102–110 (2010).
18. B. T. Vu, N. T. Dang, T. C. Thang, and A. T. Pham, "Bit error rate analysis of rectangular QAM/FSO systems using an APD receiver over atmospheric turbulence channels," J. Opt. Commun. Netw. **5**, 437–446 (2013).
19. S. Harjeevan and M. Rajan, "Performance analysis of terrestrial free space optical (FSO) communication link using M-QAM modulation technique," Int. J. Sci. Eng. Res. **4**, 805–808 (2013).
20. F. J. Escribano and A. Wagemakers, "Performance analysis of QAMMPPM in turbulence-free FSO channels: accurate derivations and practical approximations," IEEE Syst. J. **15** 1753–1763 (2020).
21. P. K. Singya, N. Kumar, V. Bhatia, and M. S. Alouini, "On the performance analysis of higher order QAM schemes over mixed RF/FSO systems," IEEE Trans. Veh. Technol. **69**, 7366–7378 (2020).
22. Y. Chen, M. Kong, T. Ali, J. Wang, R. Sarwar, J. Han, C. Guo, B. Sun, N. Deng, and J. Xu, "26 m/5.5 Gbps airwater optical wirelesscommunication based on an OFDM-modulated 520-nm laser diode," Opt. Express **25**, 14760–14765 (2017).
23. L. Kadhim, "16/64QAM modulation technique for free space optical communication system," Int. J. Adv. Comput. Technol. **6**, 1–13 (2014).
24. F. Wang, Y. Zhao, and N. Chi, "High speed visible light communication system using QAM-DMT modulation based on digital zero-padding and differential receiver," in *16th International Conference on Optical Communications and Networks (ICOCN)* (2017), pp. 1–3.
25. L. Zhang, H. Wang, X. Zhao, F. Lu, X. Zhao, and X. Shao, "Experimental demonstration of a two-path parallel scheme for M-QAM-OFDM transmission through a turbulent-air-water channel in optical wireless communications," Opt. Express **27**, 6672–6688 (2019).
26. L. C. Andrews and R. L. Phillips, *Laser Beam Propagation Through Random Media*, 2nd ed. (2005).
27. X. Li, T. Geng, S. Ma, Y. Li, S. Gao, and Z. Wu, "Performance improvement of coherent free-space optical communication with quadrature phase-shift keying modulation using digital phase estimation," Appl. Opt. **56**, 4695–4701 (2017).
28. R. J. Noll, "Zernike polynomials and atmospheric turbulence," J. Opt. Soc. Am. **66**, 207–211 (1976).
29. A. Belmonte and J. M. Khan, "Performance of synchronous optical receivers using atmospheric compensation techniques," Opt. Express **16**, 14151–14162 (2008).
30. A. Belmonte and J. M. Khan, "Capacity of coherent free-space optical links using diversity-combining techniques," Opt. Express **17**, 12601–12611 2009.
31. D. L. Fried, "Optical heterodyne detection of an atmospherically distorted signal wave front," Proc. IEEE **55**, 57–77 (1967).
32. D. S. Ly-Gagnon, S. Tsukamoto, K. Katoh, and K. Kikuchi, "Coherent detection of optical quadrature phase-shift keying signals with carrier phase estimation," J. Lightwave Technol. **24**, 12–21 (2006).